applied sciences

MDPI

Article

Precise Measurement of Hyperfine Structure of Cesium $7S_{1/2}$ Excited State

Yunhui He [1,2], Jiabei Fan [1,2], Liping Hao [1,2], Yuechun Jiao [1,2] and Jianming Zhao [1,2,*]

1 State Key Laboratory of Quantum Optics and Quantum Optics Devices, Institute of Laser Spectroscopy, Shanxi University, Taiyuan 030006, China; He_Yunhui@163.com (Y.H.); fan_jiabei@163.com (J.F.); hao_lping@163.com (L.H.); ycjiao@sxu.edu.cn (Y.J.)

2 Collaborative Innovation Center of Extreme Optics, Shanxi University, Taiyuan 030006, China

* Correspondence: zhaojm@sxu.edu.cn

Received: 29 November 2019; Accepted: 7 January 2020; Published: 10 January 2020

Abstract: We present a precise measurement of the hyperfine structure of cesium $7S_{1/2}$ excited state by employing electromagnetically induced spectroscopy (EIS) with a cesium three-level cascade ($6S_{1/2} - 6P_{3/2} - 7S_{1/2}$) atom in a room temperature vapor cell. A probe laser, λ_p = 852 nm, was coupled to a transition $|6S_{1/2}\rangle \rightarrow |6P_{3/2}\rangle$, related frequency locked to the resonance hyperfine transition of $|6S_{1/2}\rangle \rightarrow |6P_{3/2}\rangle$ with a Fabry–Perot (FP) cavity and an electro-optic modulator (EOM). A coupling laser, λ_c = 1470 nm, drove the $|6P_{3/2}\rangle \rightarrow |7S_{1/2}\rangle$ transition with the frequency scanned over the $|6P_{3/2}\rangle \rightarrow |7S_{1/2}\rangle$ transition line. The hyperfine level interval was extracted to be 2183.61 ± 0.50 MHz by analyzing EIS spectroscopy. The optical–optical double-resonance (OODR) spectroscopy is also presented for comparison, with the corresponding value of the hyperfine level interval being 2183.48 MHz ± 0.04 MHz, and the measured hyperfine splitting of excited $7S_{1/2}$ state is shown to be in excellent agreement with the previous work.

Keywords: hyperfine structure; electromagnetically induced spectroscopy; cesium $7S_{1/2}$ excited state

1. Introduction

With fast development of high-resolution spectroscopy and laser technique, fundamentally important atom-based precise measurements, such as electric field and basic physical constant, are receiving growing attention in the communities of quantum optics, quantum information, and atomic physics. Atom-based metrology has had a tremendous impact on science, technology, and everyday life. Seminal advances include optical atomic clocks [1,2], the Global Positioning System, and highly sensitive, position-resolved magnetometers. Atom-based measurements have clear advantages due to the invariance of atomic properties. Therefore, precise measurements of atomic hyperfine structures play an important role in better understanding the atomic structure and its characteristics. Hyperfine structures are caused by the interaction between the nuclear spin and electron angular momentum. Due to having one outermost electron that is similar to hydrogen, alkali metals are one of the most popular groups of elements to study in both theory and experiment. This feature provides theorists with tractable calculations and experimentalists access to the atom's structure through optical and microwave sources. The study of hyperfine structures has great influences on parity non-conservation [3,4], laser cooling and trapping of atoms [5], high-resolution spectroscopy [6], and frequency reference [7,8]. Precise measurements of atomic hyperfine structure can: (i) inspect the accuracy of fundamental physics issues theoretically; and (ii) provide a more precise frequency reference experimentally.

The investigation of the hyperfine structure for alkali metal atoms is always attractive in atomic physics. Before preceding, we note that a few groups have carried out experiments on the hyperfine

structure of the alkali metal atoms. Gilbert et al. [9] investigated the hyperfine structure of Cs $|7S_{1/2}\rangle$ state by laser excitation of $|6S_{1/2}\rangle \rightarrow |7S_{1/2}\rangle$ transition within the electric field. Stalnaker et al. [10] measured the absolute frequencies and the hyperfine coupling constant of Cs atoms by using a femtosecond frequency comb. Kiran Kumar et al. [11] measured the hyperfine splitting of Cs $|9S_{1/2}\rangle$ using Doppler-free two-photon fluorescence spectroscopy. Yang et al. [12] determined the hyperfine coupling constant of Cs $|7S_{1/2}\rangle$ state by optical–optical double-resonance spectroscopy (OODR).

Different from the previous studies [9–12], we investigated the hyperfine splitting of cesium $|7S_{1/2}\rangle$ state by using electromagnetically induced spectroscopy (EIS) in the three-level cascade atomic system, consisting of $|6S_{1/2}\rangle$, $|6P_{3/2}\rangle$, and $|7S_{1/2}\rangle$ states, where the probe laser couples the $|6S_{1/2}\rangle \rightarrow |6P_{3/2}\rangle$ transition and coupling laser drives the $|6P_{3/2}\rangle \rightarrow |7S_{1/2}\rangle$ transition. We used the hyperfine level interval of $|6P_{3/2}\rangle$ state, which is well known, as a standard frequency reference to determine the $|7S_{1/2}\rangle$ hyperfine structure. Furthermore, we present the measurement by OODR spectroscopy. Both EIS and OODR are shown to be in excellent agreement with the previous measurements [10,12] and the theoretical calculations [13].

2. Experimental Setup

We considered a three-level cesium atomic system with a ladder-type level configuration, as shown in Figure 1. An 852 nm laser coupled the ground state $|6S_{1/2}\rangle$ and intermediate state $|6P_{3/2}\rangle$, and a 1470 nm laser coupled state $|6P_{3/2}\rangle$ and an excited state $|7S_{1/2}\rangle$. Figure 1 (right) displays the hyperfine levels and relative splittings of $|6S_{1/2}\rangle$ and $|6P_{3/2}\rangle$ referring to the work of Steck [14]. Considering the nuclear spin of Cs atom I=7/2, the $|S_{1/2}\rangle$ state splits into hyperfine doublets, and the $|6P_{3/2}\rangle$ level splits into four hyperfine levels, displayed with the quantum number F. According to the selection rule, five transitions from the ground hyperfine level $|6S_{1/2}(F=4)\rangle$ are allowed, which are indicated by arrows on the right-hand side of Figure 1. For simplicity, we denote the transition by hyperfine quantum number, i.e., the transition $|6S_{1/2}(F=4)\rangle \rightarrow |6P_{3/2}(F'=3)\rangle \rightarrow |7S_{1/2}(F''=4)\rangle$ is denoted as $F=4-F'=3-F''=4$ or simply 4-3-4.

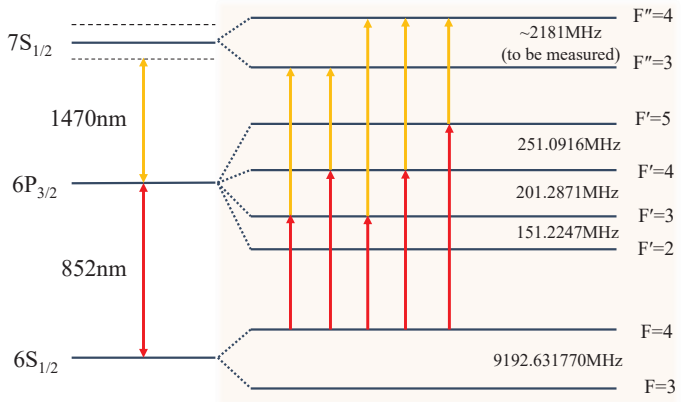

Figure 1. (color online) Three-level energy scheme. An 852 nm laser couples the transition of $|6S_{1/2}\rangle \rightarrow |6P_{3/2}\rangle$, while 1470 nm laser drives $|6P_{3/2}\rangle \rightarrow |7S_{1/2}\rangle$ transition. The right panel displays the hyperfine levels. The hyperfine level intervals of the ground and intermediate state refer to Steck [14]. The arrows display possible transitions of $|6S_{1/2}(F=4)\rangle$ ground hyperfine level.

The experiments were performed in a room temperature cesium vapor cell with diameter 25 mm and length 75 mm. The cell is made of silica glass. The related apparatus is shown in Figure 2. Two lasers, λ_p = 852 nm and λ_c = 1470 nm, were used to couple the lower and upper transitions. The 852 nm laser was provided by a diode laser (DL pro, Toptica); the related frequency was locked

to the first side band of an electro-optic modulator (EOM) employing PDH (Pound–Drever–Hall) method with an ultra-stable Fabry–Perot (FP) cavity of a finesse 15,000. The frequency was then tuned to the resonant hyperfine transition of $|6S_{1/2}(F)\rangle \rightarrow |6P_{3/2}(F')\rangle$ by changing the radio-frequency that was applied to an EOM, monitored with a wavelength meter (WS-U,HighFinesse GmbH). The 1470 nm laser, provided from the other DLpro diode laser, was scanned over the $|6P_{3/2}\rangle \rightarrow |7S_{1/2}\rangle$ transition, calibrated with a FP cavity (SA200-12B, Thorlabs). Two lasers were lined and overlapped in a counter-propagating geometry inside two separated cesium vapor cells. The purple square in Figure 2 indicates the experimental setup for an EIS measurement, while the red square denotes the setup for an OODR measurement. For the EIS measurement, the 852 nm beam probe was passed through a dichroic mirror (DM1) and detected with a photodiode (PD1). For the OODR measurement, the 1470 nm beam was detected with a balanced photodiode detector (BPD). The PD2 was employed to monitor the 1470-nm laser power.

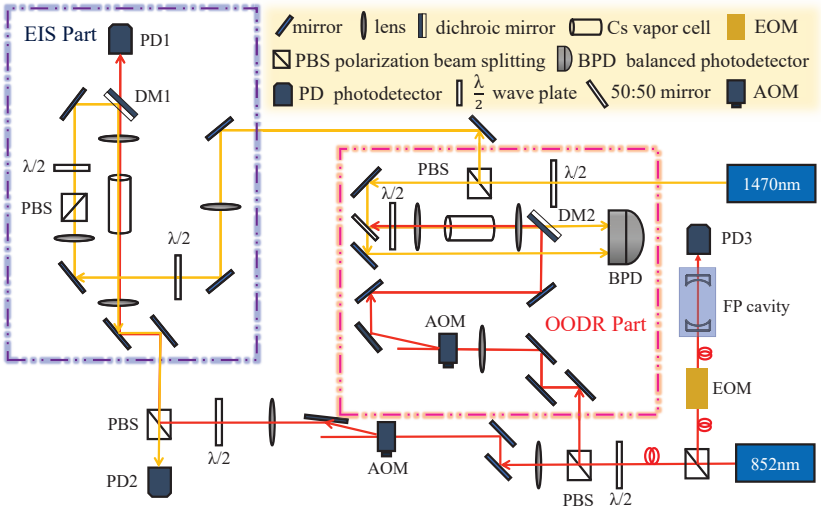

Figure 2. (color online) Layout of the experimental setup. The 852 and 1470 nm lasers couple the lower and upper transitions and are set to overlap in a counter-propagating geometry inside two separated 75-mm-long Cs room-temperature vapor cells. The purple square indicates the setup of the EIS measurement, where the probe power is detected with a photodiode detector (PD1) after passing through a dichroic mirror (DM1). The red square denotes the setup of the OODR measurement, where the 1470 nm beam is detected with a balanced photodiode detector (BPD) after passing through the other dichroic mirror DM2. In the setup, the probe laser power is kept fixed by using a PID (proportional integral derivative) feedback loop that controls the RF power supplied to an AOM (acousto-optic modulator). The probe frequency is locked to the first side band of an electro-optic modulator (EOM) employing PDH (Pound–Drever–Hall) method with an ultra-stable Fabry–Perot (FP) cavity of a finesse 15,000. The PD2 is used to monitor the 1470 nm laser power.

3. Results

We measured the hyperfine splitting of $|7S_{1/2}\rangle$ state employing two different methods, EIS spectroscopy and OODR spectroscopy. The EIS displayed two typical phenomenons, i.e., electromagnetically induced transparency (EIT) and electromagnetically induced absorption (EIA), for coupling laser detuning Δ_c (see Figure 3). EIT (EIA) is a quantum elimination (constructive) interference among excitation pathways in the three-level atom that led to a cancellation (enhancement) of absorption in the medium. The OODR spectroscopy is an optical resonant spectroscopy that is widely used to investigate the excited state [11,12]. Below, we present the EIS and OODR spectroscopy to study the hyperfine structure of cesium $|7S_{1/2}\rangle$ state.

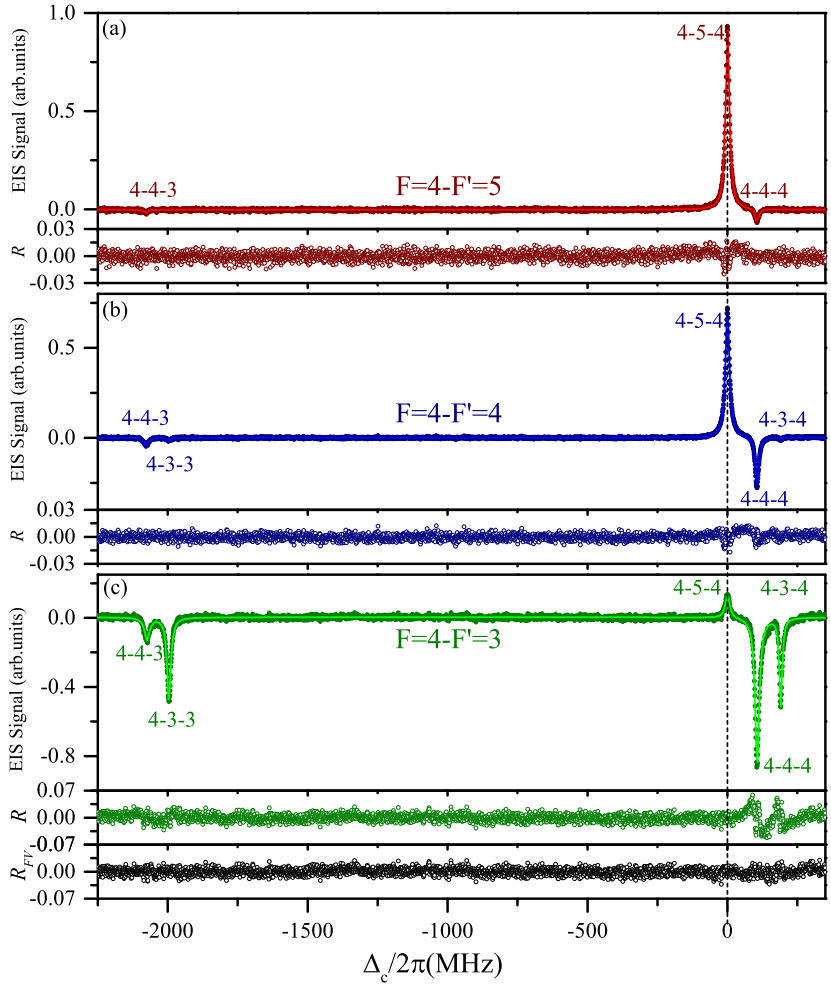

Figure 3. (color online) EIS spectroscopy for the probe laser locked to the transitions: $F = 4 - F' = 5$ (**a**); $F = 4 - F' = 4$ (**b**); and $F = 4 - F' = 3$ (**c**) . The coupling laser scanned cover the $|6P_{3/2}\rangle \rightarrow |7S_{1/2}\rangle$ transition. Solid lines display the Lorentz fittings to EIS spectra for extracting the position of EIS peaks and further the hyperfine splitting. The bottom curves display the residuals, R, of the Lorentzian fit and spectrum. The label R_{FV} at the bottom of (**c**) displays the residuals of the Fano–Vogit fit and the spectrum.

3.1. Electromagnetically Induced Spectroscopy

In EIS experiments, a probe (coupling) laser has a power of 3 µW (16 µW) and a beam waist of $\omega_{852} \simeq 100$ µm ($\omega_{1470} \simeq 150$ µm). The weak power of probe (coupling) laser results in a negligible line broadening. The coupling and probe beams are linear polarized along the vertical direction. The probe transmission is detected as a function of the coupling laser detuning Δ_c. In Figure 3, we display EIS spectra for the probe laser frequency locked to the $|6S_{1/2}(F = 4)\rangle \rightarrow |6P_{3/2}(F' = 3, 4, 5)\rangle$ hyperfine transitions, while coupling laser scanned cover the $|6P_{3/2}\rangle \rightarrow |7S_{1/2}\rangle$ transition. The spectra demonstrate some EIT or EIA peaks corresponding to the possible transitions labeled in Figure 1. To analyze and measure the hyperfine splitting of $|7S_{1/2}\rangle$ state from EIS spectra, we defined the EIS peak of 4-5-4 as the zero-detuning point and calibrate coupling laser detuning, Δ_c, with the space between EIS 4-5-4 and 4-4-4 peaks due to the accurate hyperfine splitting of $|6P_{3/2}\rangle$ state [14]. Considering the Doppler factor, the EIS peak distance between 4-5-4 and 4-4-4 peaks is $251.09 \times (1 - 852/1470)$ = 105.56 MHz and 4-4-4 peak is located on the blue side. Besides, we calibrated the coupling laser detuning using high order side band of EOM to decrease the effect of the nonlinearity of coupling frequency during the laser scanning. Moreover, we used Lorentz function to fit each peak to extract the peak positions and further the hyperfine structure splitting of $|7S_{1/2}\rangle$ state.

Figure 3 presents the EIS spectroscopies for the probe laser locking to the indicated hyperfine transitions. Figure 3 shows that the EIS spectra present different profiles for probe frequency locked to different hyperfine transitions. Among three cases of probe frequency, only the 4-5-4 peak displays the decrease of probe absorption, i.e., EIT spectrum, because the 4-5-4 configuration constitutes the cycling transition. The 4-5-4 peak displays strong EIT signal when the probe laser resonantly interacts with the $F = 4 - F' = 5$ hyperfine transition (see Figure 3a) and shows decreased EIT when probe laser locked to $F = 4 - F' = 4$ hyperfine transition due to the detuned interaction of probe for the 4-5-4 configuration (see Figure 3b). The 4-5-4 peak displays the smallest EIT signal when the probe frequency is locked to the $F = 4 - F' = 3$ hyperfine transition due to larger detuning for the 4-5-4 configuration (see Figure 3c). All other EIS peaks show increase of the probe absorption, i.e., EIA spectrum, as the other four configurations are non-cycling transition and a large population leakage occurs via spontaneous emission decays from the excited state to the other ground states [15].

We take the case of probe locked to $F = 4 - F' = 4$ (Figure 3b) as an example to illustrate how we obtained the hyperfine splitting of excited $|7S_{1/2}\rangle$ state. The spectrum of probe locked to $F = 4 - F' = 4$ clearly shows the five indicated transition signals, where one of them is an EIT signal of the 4-5-4 cycling transition and the others are EIA signals of non-cycling transitions. The 4-4-4 and 4-3-4 peaks sit on the blue side originating from the hyperfine level of $|7S_{1/2}(F'' = 4)\rangle$, whereas 4-4-3 and 4-3-3 EIA peaks are on the red side coming from the contributions of hyperfine level of $|7S_{1/2}(F'' = 3)\rangle$. The positions of EIA peaks were attained by Lorentz fittings to the EIA signals, as displayed with solid lines in Figure 3. From the separation between 4-4-4 and 4-4-3 (4-3-4 and 4-3-3) peaks, we attained the hyperfine splitting of $7S_{1/2}$ of 2184.18 $\pm$ 0.26 MHz with 2σ error of five independent measurements. Similar analyses of the spectra in Figure 3a,c yielded the hyperfine splittings of 2183.16 $\pm$ 0.35 MHz (Figure 3a) and 2183.51 $\pm$ 0.08 MHz (Figure 3c), respectively. The average of three cases yielded the hyperfine splitting 2183.61 $\pm$ 0.50 MHz of excited $|7S_{1/2}\rangle$ state.

To investigate the line shape distortion and further the energy shift caused by quantum interference [16,17], as shown at the bottom of Figure 3a–c, we present the residuals, R, of the Lorentzian fits and spectra. The residuals demonstrate the small deviation of 4-5-4 peak in Figure 3a and the 4-4-4 peak in Figure 3b, but a larger deviation of 4-4-4 and 4-3-4 peaks in Figure 3c. We fitted the spectrum in Figure 3c with the Fano–Vogit function to analyze the line shape distortion induced by the quantum interference. The corresponding residuals of the Fano–Vogit fits and spectrum are labeled with R_{FV} at the bottom of Figure 3c. The estimated shift due to the quantum interference is $\lesssim$100 kHz.

3.2. OODR Spectroscopy

The OODR measurement is a popular technique for high-resolution spectroscopy and has been widely employed for investigating the hyperfine structure of the excited state and transitions between excited states of atoms or molecules [18,19]. The details of OODR are shown in [12]. For comparison with EIS measurements above, we also present OODR spectroscopy measurements of the hyperfine interval of $|7S_{1/2}\rangle$ state. The experimental setup of OODR measurement is indicated by the red square in Figure 2. The first step excitation comes from the 852 nm laser with a power 5 µW before entering the vapor cell, with related waist $\omega_{852} \simeq 150$ µm. The first step laser power was larger than that of the EIS experiments to populate enough atoms in the intermediate $6P_{3/2}$ state. The second step excitation was driven by 1470 nm laser with power $\sim$16 µW and waist $\omega_{1470} \simeq 400$ µm in the cell center. The 1470 nm laser passed through the dichroic mirror (DM2) and was detected with a balanced photodiode detector (BPD). To avoid the power fluctuation during the frequency scanning, the 1470 nm laser was separated into two parts, where one was measured by OODR spectroscopy and the other propagated through a similar route as the first one but without overlapping with first step beam. We used the difference of the two 1470-nm parts as the final OODR spectroscopy.

In Figure 4, we present the OODR spectroscopies for the first step excitation laser locked to $|6S_{1/2}(F = 4)\rangle \rightarrow |6P_{3/2}(F' = 3, 4, 5)\rangle$ hyperfine transitions. For the first step locked to $F = 4 - F' = 4$ (Figure 4b) and $F = 4 - F' = 3$ (Figure 4c) cases, we clearly observed five double resonant peaks,

corresponding to the five possible transitions in Figure 1. For the $F = 4 - F' = 5$ case (Figure 4a), only three double resonant peaks were attained due to the selective rule. We defined the OODR peak of 4-5-4 as the zero-detuning of second step excitation. The Lorentz fittings to the OODR peaks yielded the peak positions and the hyperfine splitting of $7S_{1/2}$ (see solid lines in Figure 4). We used a similar method to extract the hyperfine splitting of $|7S_{1/2}\rangle$ state 2183.46 ± 0.04 MHz (Figure 4a), 2183.46 ± 0.18 MHz (Figure 4b), and 2183.53 ± 0.10 (Figure 4c). The average of the three cases yielded the hyperfine splitting 2183.48 ± 0.04 MHz of excited $|7S_{1/2}\rangle$ state. Similar to EIS, we also show the residuals of the Lorentz fits and spectra at the bottom of Figure 4a–c.

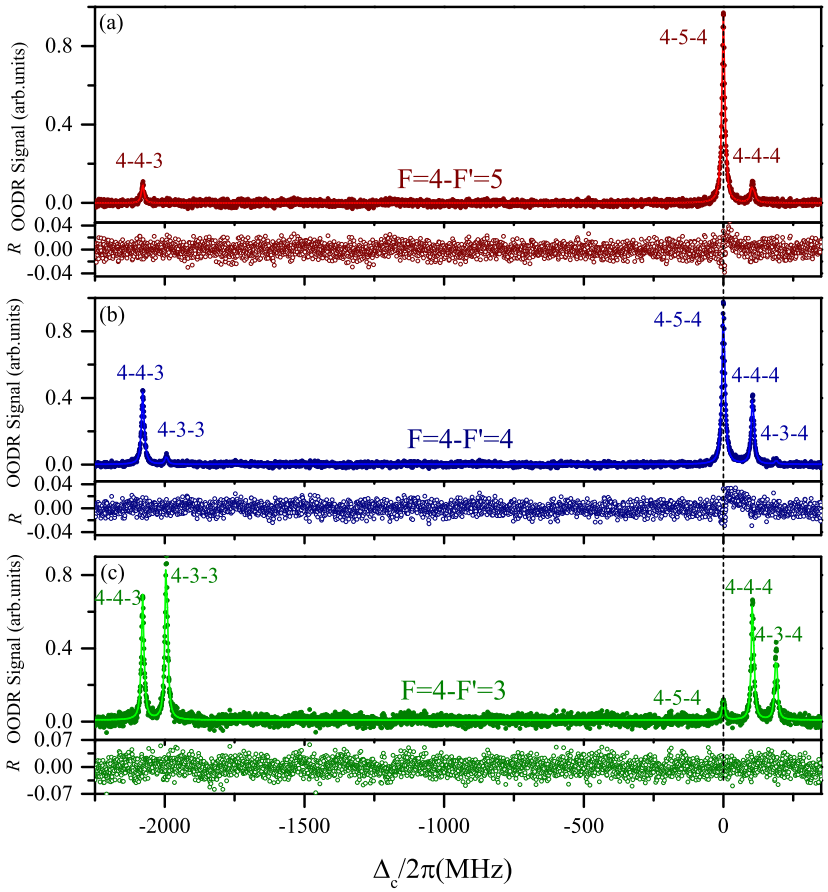

Figure 4. (color online) Measurements of OODR spectroscopy for first step laser locked to the hyperfine transitions: $F = 4 - F' = 5$ (**a**); $F = 4 - F' = 4$ (**b**); and $F = 4 - F' = 3$ (**c**). The spectroscopy displays five indicated double resonant peaks, labeled with arrows in Figure 1. The solid lines are Lorentz fittings to the double resonant peaks. The bottom curves show the residuals, *R*, of the Lorentz fits and spectra.

4. Discussions and Conclusions

We used EIS and OODR spectra to investigate the hyperfine structure of cesium $|7S_{1/2}\rangle$ excited state. The measured hyperfine splitting is displayed in Table 1. To compare with the previous results, we also display the calculated and measured hyperfine splittings mentioned in [9,12,13,20]. The measured hyperfine splitting is 2183.61 ± 0.50 MHz by EIS and 2183.48 ± 0.04 MHz by OODR in this work, showing a good agreement with the previous experimental measurements in [9,12] and the calculation by Kheteslius [13]. We found that the two methods can obtain the same results. One can see that the EIS measurement has three obvious advantages: (i) EIS spectroscopy is a quantum effect that needs weak probe laser power; (ii) the probe frequency locking to hyperfine transition leads to the Doppler-free narrow linewidth signal; and (iii) the weak probe could decrease the atomic population at intermediate $|6P_{3/2}\rangle$ level, therefore the radiation decay effect on the EIS can be effectively compressed.

We finally discuss the error of measurements, which might be contributed by the following reasons. (i) The main reason causing the error is nonlinearity of the coupling laser frequency scanning. To measure hyperfine splitting of $7S_{1/2}$ state, the 1470 nm laser needs to scan over $\gtrsim$2.3 GHz and the minor nonlinearity of frequency scanning could lead to error. (ii) The error could also come from the frequency calibration of 1470 nm laser. We used hyperfine splitting of cesium $|6P_{3/2}\rangle$ in EIS or OODR spectrum and another wavelength meter (WS-6, HighFinesse GmbH) to calibrate the 1470-nm laser. A saturated absorption spectra and the wavelength meter (WS-U, HighFinesse GmbH) were used to calibrate the 852 nm frequency. (iii) Moreover, the error could come from fitting to signal peak. We used Lorentz fittings to EIS or OODR peaks and extracted the peak position. For the EIS measurements, the fittings to the spectra would yield a systematic error (see the residuals in Figure 3). This kind of error can be further decreased by modeling the measurement using a density matrix formalism [16,17] and the corresponding accuracy is expected to be further improved. (iv) The laser power broadening and shift may also induce an error, which would be negligible due to very smaller laser power used in our study.

Table 1. Comparison of hyperfine splitting of $|7S_{1/2}\rangle$ excited state measured using EIS and OODR spectroscopy in this work with the previous theoretical calculations and measurements.

Reference	7S Hyperfine Splitting (MHz)
Dzuba [20]	2246.04 (theory)
Kheteslius [13]	2181.92 (theory)
Gilbert [9]	2183.60(36) (experiment)
Yang [12]	2183.273(062) (experiment)
This work by OODR	2183.48(04)
This work by EIS	2183.61(50)

In summary, we measured hyperfine splitting of cesium $|7S_{1/2}\rangle$ state using EIS spectroscopy employing the $6S_{1/2} - 6P_{3/2} - 7S_{1/2}$ cascade transitions in a room temperature vapor cell. EIS spectrum was attained by detecting a weak probe laser that was locked to the lower hyperfine transition. This kind of spectra is Doppler-free and with narrow linewidth. The $|7S_{1/2}\rangle$ state hyperfine splitting we measured by electromagnetic induced spectrum is 2183.61 $\pm$ 0.50 MHz, while the OODR measurement is 2183.48 MHz $\pm$ 0.04 MHz. The measurements are in good agreements with theoretical calculations [13] and previous experiments. In the future, we will model the measured spectrum using a density matrix formalism to decrease the systematic error and use a high finesse cavity for calibrating the up transition laser to realize precise measurement of the excited state.

Author Contributions: Conceptualization, Y.H. and J.Z.; investigation, Y.H., J.Z., and Y.J.; software, Y.J., J.F.; validation, Y.H., L.H., and J.F.; formal analysis, Y.H., J.F., and L.H.; Writing—original draft, Y.H.; writing—review and editing, J.Z.; project administration, J.Z. and Y.J.; and funding acquisition, J.Z. and Y.J. All authors have read and agreed to the published version of the manuscript.

Funding: We thank Zhengyang Bai for reading through the manuscript. The work was supported by the National Key R&D Program of China (Grant No. 2017YFA0304203), the National Natural Science Foundation of China (Grants Nos. 11434007, 61835007, 61675123, 61775124, and 11804202), Changjiang Scholars and Innovative Research Team in University of Ministry of Education of China (Grant No. IRT_17R70), and 1331 project.

Conflicts of Interest: The authors declare no conflict of interest.

References

1. Boyd, M.M.; Ludlow, A.D.; Blatt, S.; Foreman, S.M.; Ido, T.; Zelevinsky, T.; Ye, J. ^{87}Sr Lattice Clock with Inaccuracy below 10^{-15}. *Phys. Rev. Lett.* **2007**, *98*, 083002. [CrossRef] [PubMed]
2. Bloom, B.J.; Nicholson, T.; Williams, J.R.; Campbell, S.L.; Bishof, M.; Zhang, X.; Zhang, W.; Bromley, S.L.; Ye, J. An optical lattice clock with accuracy and stability at the 10^{-18} level. *Nature* **2014**, *506*, 71–75. [CrossRef] [PubMed]

3. Wood, C.S.; Bennett, S.C.; Cho, D.; Masterson, B.P.; Roberts, J.L.; Tanner, C.E.; Wieman, C.E. Measurement of parity nonconservation and an anapole moment in Cesium. *Science* **1997**, *275*, 1759–1763. [CrossRef] [PubMed]
4. Kozlov, M.G.; Porsev, S.G. High-accuracy calcalation of $6S \rightarrow 7S$ parity-nonconserving amplitude in Cs. *Phys. Rev. Lett.* **2001**, *86*, 3260. [CrossRef] [PubMed]
5. Magno, W.C.; Cavasso Filho, R.L.; Cruz, F.C. Two-photon Doppler cooling of alkaline-earth-metal and ytterbium atoms. *Phys. Rev. A* **2003**, *67*, 043407. [CrossRef]
6. Hollberg, L.; Hall, J.L. Measurement of the Shift of Rydberg Energy Levels Induced by Blackbody Radiation. *Phys. Rev. Lett.* **1984**, *53*, 230. [CrossRef]
7. Sasada, H. Wavenumber measurements of sub-Doppler spectral lines of Rb at 1.3 μm and 1.5 μm. *IEEE Photonics Technol. Lett.* **1992**, *4*, 1307–1309. [CrossRef]
8. Gupta, R.; Happer, W.; Lam, L.K.; Svanberg, S. Hyperfine-structure measurements of excited S states of the stable isotopes of potassium, rubidium, and cesium by cascade radio-frequency spectroscopy. *Phys. Rev. A* **1973**, *8*, 2792. [CrossRef]
9. Gilbert, S.L.; Watts, R.N.; Wieman, C.E. Hyperfine-structure measurement of the 7S state of cesium. *Phys. Rev. A* **1983**, *27*, 581. [CrossRef]
10. Stalnaker, J.E.; Mbele, V.; Gerginov, V.; Fortier, T.M.; Diddams, S.A.; Hollberg, L.; Tanner, C.E. Femtosecond frequency comb measurement of absolute frequencies and hyperfine coupling constants in cesium vapor. *Phys. Rev. A* **2010**, *81*, 043840. [CrossRef]
11. Kiran Kumar, P.V.; Suryanarayana, M.V. Measurement of the hyperfine splitting of the $9S_{1/2}$ level in Cesium by Doppler-free two-photon spectroscopy. *Opt. Commun.* **2012**, *285*, 1838–1842. [CrossRef]
12. Yang, G.; Wang, J.; Yang, B.D.; Wang, J.M. Determination of the hyperfine coupling constant of the cesium $7S_{1/2}$ state. *Laser Phys. Lett.* **2016**, *13*, 085702. [CrossRef]
13. Khetselius, O.Y. Relativistic calculation of the hyperfine structure parameters for heavy elements and laser detection of the heavy isotopes. *Phys. Scr.* **2009**, *T135*, 014023. [CrossRef]
14. Steck, D.A. Cesium D Line Data. Available online: http://steck.us/alkalidata (accessed on 8 January 2020).
15. Failache, H.; Valente, P.; Ban, G.; Lorent, V.; Lezama, A. Inhibition of electromagnetically induced absorption due to excited-state decoherence in Rb vapor. *Phys. Rev. A* **2003**, *67*, 043810. [CrossRef]
16. Beyer, A.; Maisenbacher, L.; Matveev, A.; Pohl, R.; Khabarova, K.; Grinin, A.; Lamour, T.; Yost, D.C.; Hansch, T.W.; Kolachevsky, N.; et al. The Rydberg constant and proton size from atomic hydrogen. *Science* **2017**, *358*, 79–85. [CrossRef] [PubMed]
17. Marsman, A.; Horbatsch, M.; Hessels, E.A. Shifts due to distant neighboring resonances for laser measurements of 2^3S_1-to-2^3P_J transitions of helium. *Phys. Rev. A* **2012**, *86*, 040501. [CrossRef]
18. Boucher, R.; Breton, M.; Cyr, N.; Têtu M. Dither-free absolute frequency locking of a 1.3μm DFB laser on ^{87}Rb. *IEEE Photonics Technol. Lett.* **1992**, *4*, 327–329. [CrossRef]
19. Loftus, T.; Bochinski, J.R.; Mossberg, T.W. Optical double-resonance cooled-atom spectroscopy. *Phys. Rev. A* **2001**, *63*, 023402. [CrossRef]
20. Dzuba, V.A.; Flambaum, V.V.; Sushkov, O.P. Relativistic many-body calculations of the hyperfine-structure intervals in caesium and francium atoms. *J. Phys. B At. Mol. Phys.* **1984**, *17*, 1953. [CrossRef]

© 2020 by the authors. Licensee MDPI, Basel, Switzerland. This article is an open access article distributed under the terms and conditions of the Creative Commons Attribution (CC BY) license (http://creativecommons.org/licenses/by/4.0/).